Demonstration of Model-Independent Control of the Longitudinal Phase Space of Electron Beams in the Linac-Coherent Light Source with Femtosecond Resolution

Alexander Scheinker,[1,*] Auralee Edelen,[2] Dorian Bohler,[2] Claudio Emma,[2] and Alberto Lutman[2]
[1]Los Alamos National Laboratory, P.O. Box 1663, Los Alamos, New Mexico 87545, USA
[2]SLAC National Accelerator Laboratory, 2575 Sand Hill Road, Menlo Park, California 94025, USA

(Received 26 February 2018; revised manuscript received 5 June 2018; published 25 July 2018)

The dynamics of intense electron bunches in free electron lasers and plasma wakefield accelerators are dominated by complex collective effects such as wakefields, space charge, coherent synchrotron radiation, and drift unpredictably with time, making it difficult to control and tune beam properties using model-based approaches. We report on a first of its kind combination of automatic, model-independent feedback with a neural network for control of the longitudinal phase space of relativistic electron beams with femtosecond resolution based only on transverse deflecting cavity measurements.

DOI: 10.1103/PhysRevLett.121.044801

Free electron lasers (FEL) and plasma wakefield accelerators (PWFA) are flexible scientific instruments, providing a wide range of beam energies and bunch lengths for various high energy physics, biology, chemistry, material science, and accelerator physics experiments. For example, the Linac-Coherent Light Source (LCLS) FEL provides users with photon energies ranging from 0.27 keV to 12 keV based on electron bunches with energies from 2.5 GeV to 17 GeV. An operating electron bunch charge can range from 20 pC to 300 pC, and the bunch duration can range from 3 fs to 500 fs to suit experimental needs [1–3]. The updated PWFA facility for advanced accelerator experimental tests (FACET-II) is planning to provide bunch charges ranging from pC to nC of either positron or electron beams at energies of 1 to 10 GeV [4].

The precise control of bunch lengths, current profiles, and energy spreads of increasingly shorter electron beams at femtosecond resolution is extremely important and challenging [5,6]. Traditional model-based approaches are severely limited by uncertain and time varying beam phase space distributions, misalignments, thermal cycling, time varying parameters, and collective effects such as space charge forces, wakefields, and coherent synchrotron radiation emitted by extremely short high current bunches. For example, reconfiguring the LCLS to a low charge mode in order to provide 3 fs bunches can take many hours of manual tuning by experienced operators and beam line physicists. Such difficulties are limiting both the complexity of beam arrangements that can be explored at these facilities and wasting limited beam time. These difficulties will only grow for future facilities running multiple accelerators, such as the LCLS-II [7], when complex schemes such as multicolor operation [8], multistage amplification [9], or self-seeding are established [10,11], or at FACET-II, which is planning on providing custom tailored current profiles for a suite of experiments with specific requirements [12].

The goal of this work was to demonstrate a novel combination of a model-independent feedback control method with a trained neural network (NN) for fast (minutes) and automatic intense electron beam phase space control. Automatic tuning of six coupled beam line components (linac phase and bunch compressor energy set points) transformed initial electron bunches of length ~300 fs to match desired ~80 fs long current profiles, while also matching desired energy spread profiles. The addition of the neural network resulted in global rather than local convergence, making the method more robust against large long-term drifts.

Our feedback approach is based on a recently developed method, analytically studied for a large class of nonlinear, time-varying dynamic systems [13,14], which has been utilized for predicting and tracking longitudinal phase space distributions at the PWFA FACET [15]. Our multivariable approach is a new, bounded extension of the classical extremum seeking method implemented in [16] in which only a single parameter was tuned for FEL laser spectrum optimization. Our method is applicable to an n-dimensional dynamic system of the form

$$\frac{d\mathbf{x}}{dt} = \mathbf{f}(\mathbf{x}, \mathbf{p}, t), \tag{1}$$

where $\mathbf{x} = (x_1, \ldots, x_n)$ are physical quantities, such as beam properties at specific locations in a particle accelerator, $\mathbf{p} = (p_1, \ldots, p_m)$ are controlled parameters, t is time, and $\mathbf{f}$ is an unknown function governing the system's dynamics. In this Letter, we simultaneously tuned six parameters, $\mathbf{p} = (p_1, \ldots, p_6)$, of the LCLS beam line as shown in Fig. 1 in red. (1) The Linac 1 (L1S) phase set point has influence on both electron bunch energy and the length change due to bunch compressor BC1. A large change of L1S due to a drift has to be corrected via a

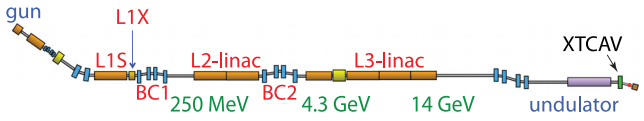

FIG. 1. Simple overview of LCLS showing the controlled parameters (in red) and XTCAV diagnostic location.

lengthy phase scan. (2) The Linac 1 X-band (L1X) cavity phase set point linearizes the electron bunch, compensating for energy curvature introduced by L1S. (3) The bunch compressor 1 (BC1) energy set point determines the amount of longitudinal compression of the bunch and provides feedback for the L1 amplitude set point. (4) The Linac 2 (L2) phase set point controls a group of multiple klystrons, effects bunch length, and suffers from the same drifts as L1. (5) The bunch compressor 2 (BC2) energy set point is a second stage of compression at higher energy. (6) The Linac 3 (L3) phase set point is another multiklystron system, subject to phase and amplitude drifts.

We minimized a measurable, analytically unknown "cost function," $C(\mathbf{x}(\mathbf{p},t),t)$, by adjusting the parameters $\mathbf{p}$ without a knowledge of the analytic form of C. Our $C(\mathbf{x}(\mathbf{p},t),t)$ was a weighted sum of the difference between measured current $\hat{\rho}_c(z)$ and energy spread profiles $\hat{\rho}_e(E)$ and desired profiles $\rho_c(z)$ and $\rho_e(E)$ at the end of the FEL, of the form

$$C(\mathbf{x}(\mathbf{p},t),t) = \int_0^L |\hat{\rho}_c(z) - \rho_c(z)|dz + 2\int_{-\Delta E}^{\Delta E} |\hat{\rho}_e(E) - \rho_e(E)|dE, \quad (2)$$

where L is a length range and $E \in [-\Delta E, \Delta E]$ is a range of electron energy. We only had access to noise corrupted measurements of C of the form

$$y(t) = C(\mathbf{x}(\mathbf{p},t),t) + n(t). \quad (3)$$

We used the x-band transverse deflecting cavity (XTCAV) to measure the beam. The XTCAV streaks the electron bunch, translating longitudinal position to transverse position. The rotated bunch is then passed through a vertical dipole causing an energy-dependent curvature of the electron trajectory. The setup is shown in Fig. 2,

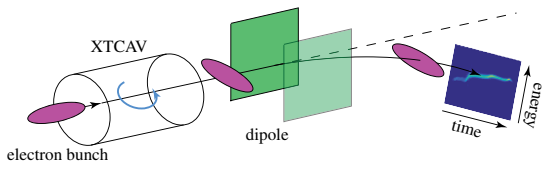

FIG. 2. Beam horizontally streaked by transverse deflecting radio frequency structures and deflected by a vertical dipole into detector, measuring current profile and energy spread.

providing both longitudinal bunch current profile and energy distribution [17].

We adjust the parameters p_j according to

$$\frac{dp_j}{dt} = \sqrt{2\alpha\omega_j}\cos(\omega_j t + ky), \quad (4)$$

where $\omega_j = \omega r_j$ and $r_j \neq r_i$ for $i \neq j$. The term $\alpha > 0$ is the dithering amplitude, and it can be increased to escape local minima. Once the dynamics have settled, a parameter p_j will oscillate about a local minimum with an amplitude $\sqrt{2\alpha/\omega_j}$. The term $k > 0$ is the feedback gain. For a large ω, the dynamics of (4) are given, on average, by the simple dynamics

$$\frac{d\mathbf{p}}{dt} = -k\alpha\nabla_{\mathbf{p}}C, \quad (5)$$

a gradient descent, with respect to $\mathbf{p}$, of the actual, analytically unknown function C, although the feedback is based only on the noisy measurements $y(t)$ [13,14]. Intuitively, the reason behind this convergence is that by dithering each parameter at a unique frequency, the evolution of the parameters has been made orthogonal in Hilbert space in the form of the $L^2[0,t]$ inner product:

$$\lim_{\omega_1,\omega_2\to\infty}\int_0^t \cos(\omega_1\tau)\cos(\omega_2\tau)d\tau = 0. \quad (6)$$

The resulting dynamics, on average, minimize a time-varying, unknown function, with many advantages over the standard gradient descent-type search: (1) Continuously, dynamically tuning many parameters of unknown, nonlinear, open-loop unstable systems, simultaneously, without exponential growth in the number of computations required. (2) The robustness to measurement noise and external disturbances, and the ability to track fast time-varying parameters. (3) Although operating on noisy and analytically unknown systems, the parameter updates have analytically guaranteed constraints: $|dp_j/dt| = |\sqrt{2\alpha\omega_j}\cos(\omega_j t + ky)| \leq \sqrt{2\alpha\omega_j}$, which is safe for in-hardware implementation.

We began by recording XTCAV distribution measurements for a fixed set of parameters, which would serve as our desired profiles $\rho_c(z)$ and $\rho_e(E)$. We then changed parameter settings, and thereby the beam's phase space distributions, and we started the algorithm in order to automatically recover the desired profiles. The procedure of applying (4) iteratively in hardware was via the finite difference approximation of (4) given by:

$$p_j(n+1) = p_j(n) + \Delta\sqrt{2\alpha\omega_j}\cos\left(\omega_j n\Delta + ky(n)\right), \quad (7)$$

which is an accurate approximation of the derivative in (4) for $\Delta < (2\pi/\max\{\omega_j\}) \ll 1$. Limits were defined for all

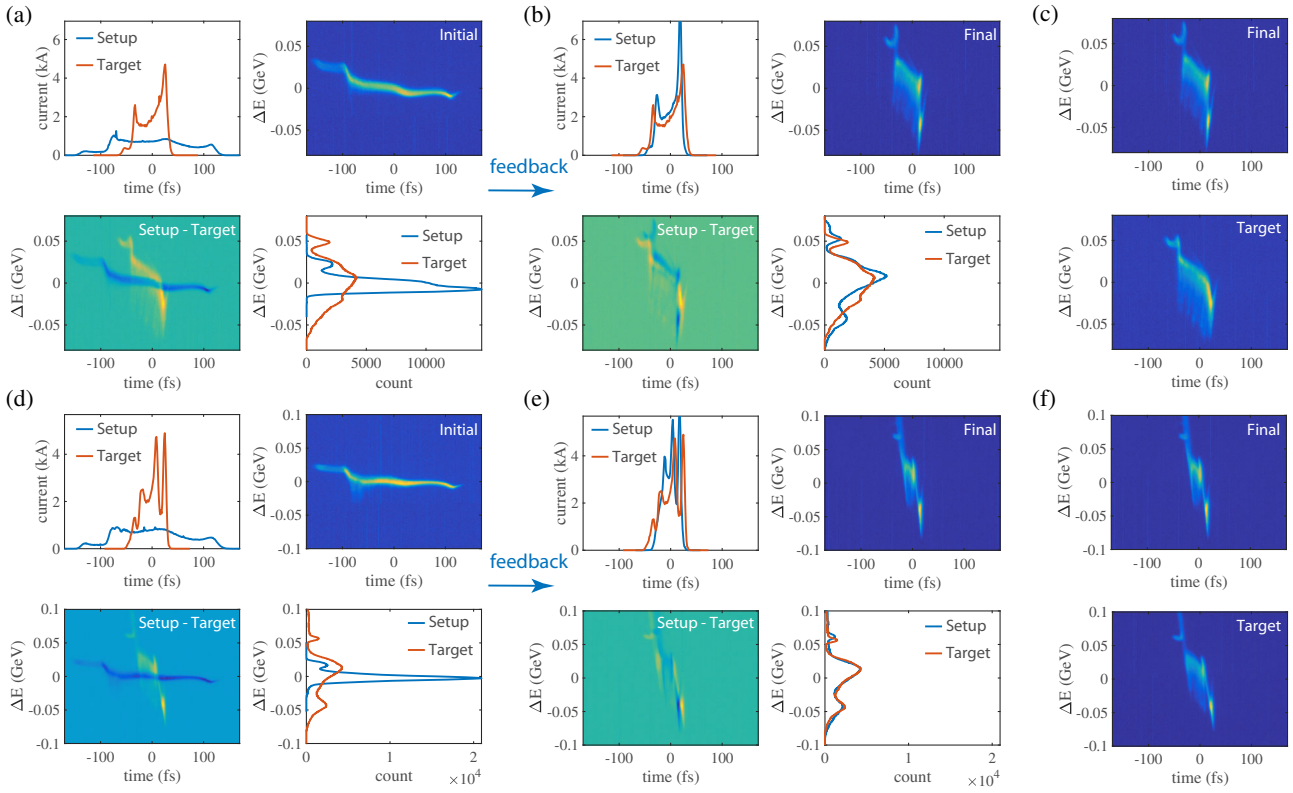

FIG. 3. (a) Experiment 1, longitudinal phase space of initial setup shown relative to target phase space (arbitrary color scale). (b) Results of running feedback. (c) Final and target phase space distributions. (d) Experiment 2, longitudinal phase space of initial setup shown relative to target phase space. (e) Results of running feedback. (f) Final and target phase space distributions.

parameters, and they were normalized to within a range of ± 1. The parameter updates were carried out on normalized values that were then unnormalized to physical set points that could be set in the LCLS. The procedure started with initial parameter settings $\mathbf{p}(1)$, after which the XTCAV image was recorded and projected on the vertical and horizontal axes. The raw measurements were smoothed with a ten-point moving average filter, and the current profile $\hat{\rho}_c(z)$ and the energy spread profile $\hat{\rho}_e(E)$ were then used to determine the cost, $C(1)$ as given by (2). Based on $C(1)$, new parameter settings $\mathbf{p}(2)$ were determined according to (7). The process was continued iteratively, at a rate of $1/4$ Hz to allow for all parameter changes to settle.

In the first experiment, the phase set point of L1S was changed by -3 deg, causing a change in both bunch length and energy spread. Figure 3 shows the desired, initial, and final longitudinal phase space distributions as achieved by the feedback. The iterative procedure then automatically tuned all six parameters to recover the desired distributions. The evolution of all parameters is shown on the left side of Fig. 4, and the evolution of the cost function is shown in Fig. 5. Although the cost function was minimized, the L1S phase did not return to its original value but was

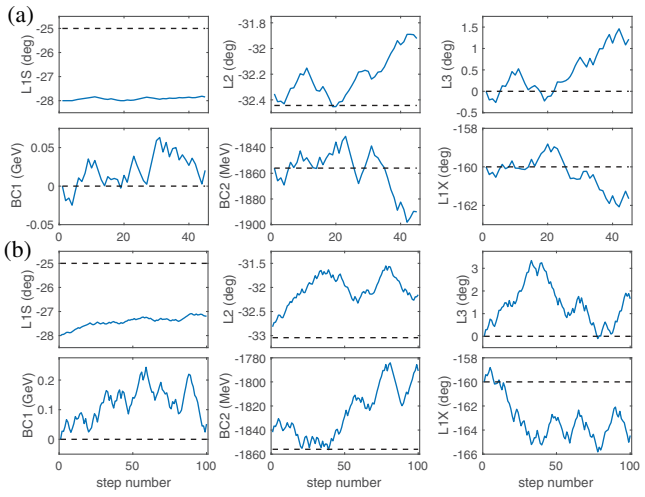

FIG. 4. Evolution of the parameters being tuned by the feedback algorithm. (a) The first experiment where only the L1S phase was changed to produce the initial beam phase space distribution. (b) The second experiment where L1S and L2 phases and BC2 energy set points were changed. Parameter settings of the target distribution are shown in black or dashed. The parameters were then changed to new starting values and the iterative process was started as shown in blue.

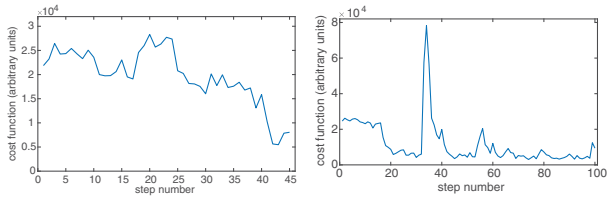

FIG. 5. Cost function of 1st (left) and 2nd (right) experiment.

compensated by changes in other parameters. Figure 3 shows the desired, initial, and final distributions, $\rho_c(z)$ and $\rho_e(E)$, based on which the cost values were calculated. The energy spread distribution has been matched almost exactly, while the current profile has recovered the correct bunch width, but it is limited in accuracy in high frequency characteristics because of the ten-point moving average that was used to clean up the profiles. Total tuning time was 3 minutes.

In a second experiment, the L1S and L2 phase and BC2 energy set points were modified, and the feedback scheme was again able to rematch the distributions by adjusting parameters as shown in Fig. 3. A large jump in the cost seen in Fig. 5 is due to a drop out of the beam, during which we kept running and recording blank XTCAV images, demonstrating the robustness of the scheme to noise and sudden step changes. The second experiment shows a better match of current profiles and a worse match in energy spread distributions. The total tuning time in the second experiment was ~6.6 minutes for 100 steps.

The next step of this work was to combine a local, model-independent feedback method with global machine learning (ML) based approaches. ML-based tools, such as NNs, can be trained to automatically tune and control large complex systems such as particle accelerators [18]. However, ML alone may be insufficient for particle accelerator systems because they are time-varying, and their learned characteristics are drifting. The ML tool must also be able to interpolate between training points, which is more difficult for complex, many-parameter systems. For the third experiment, we conducted a preliminary investigation into this approach. Because of limited beam time, we restricted ourselves to controlling two parameters: the compression ratios of BC1 and BC2. First, we performed a two-dimensional (2D) grid parameter scan while recording parameter values and TCAV images. Using these data, we

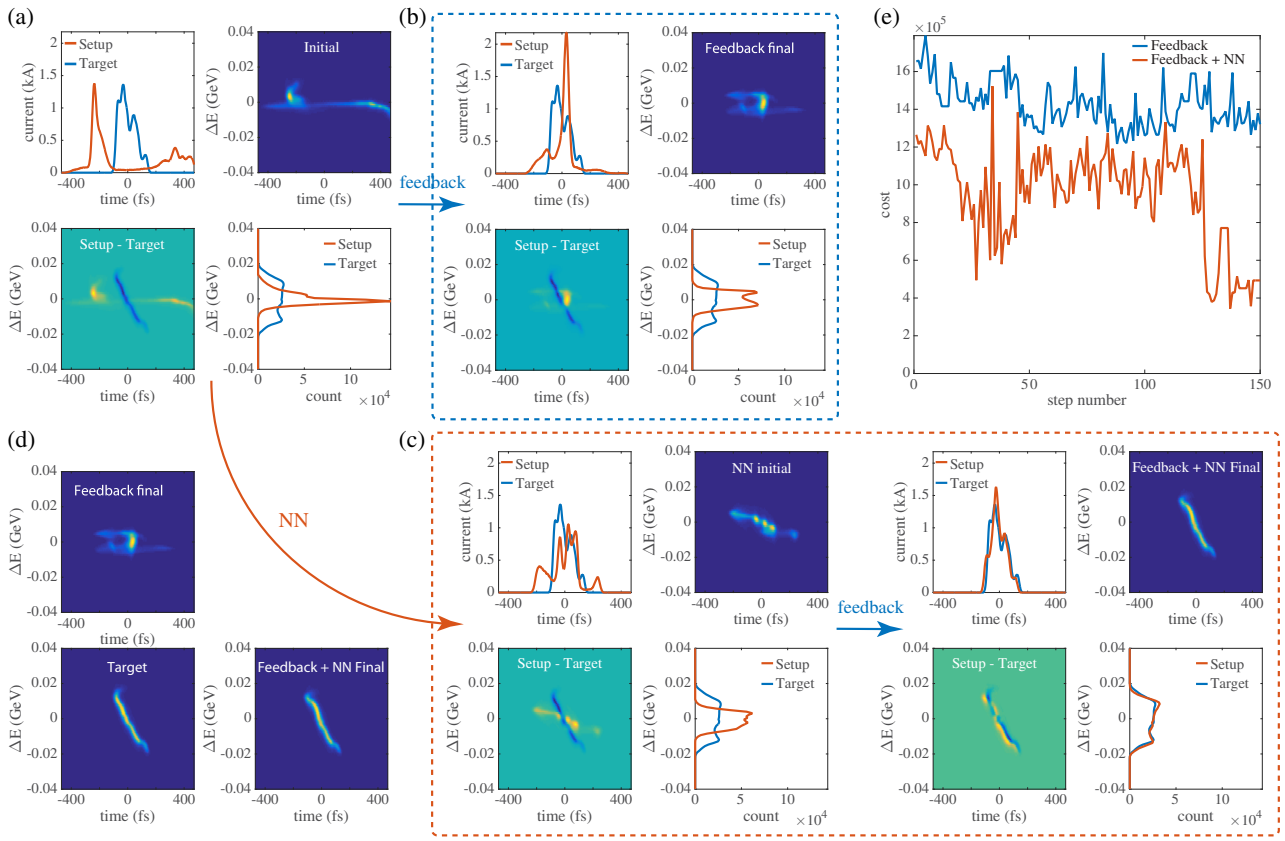

FIG. 6. (a) Longitudinal phase space of initial accelerator setup and target phase space (arbitrary color scales). (b) The parameters started very far away from their optimal values, feedback alone did not converge within 150 steps, likely stuck in a local minimum. (c) Utilizing the trained NN to give a closer initial guess, the feedback algorithm was able to converge to the desired phase space within 150 steps. (d) Final phase space distributions. (e) The cost function evolution for both cases.

TABLE I. Experiment setup details.

Experiment	Beam energy (GeV)	Bunch charge (nC)	k	α	ω	dt	Averaging	Cost function
1	4.48	0.17	1.0E-3	9	[2000, 2320, 2640, 2960, 3280, 3600]	8.7E-5	10×	1D projections
2	4.48	0.17	1.0E-3	4	[2000, 2320, 2640, 2960, 3280, 3600]	8.7E-5	10×	1D projections
3	13.42	0.18	1.4E-5	10	1000	6.3E-4	None	2D images

trained a NN to map desired phase space distributions to the parameter settings needed to achieve them. The NN itself consisted of three feed-forward hidden layers with tanh activation functions, and it was trained on 504 samples using the RMSprop optimization algorithm [19]. We demonstrated the combined feedback algorithm and NN approach by making a very large change in the parameter space and returning to a target phase space distribution that was not contained in the training data set, first with the feedback algorithm alone, and then with the combined approach. In the former case, the feedback algorithm was unable to achieve the target phase space after becoming stuck in a local minimum. The NN-based setup brought us close to the desired phase space, and the feedback was then initialized and zoomed in on the correct minimum, as shown in Fig. 6. Our cost was defined by directly comparing the machine's 2D TCAV measurement with the desired TCAV image:

$$C(\mathbf{x}(\mathbf{p},t),t) = \int_0^L \int_{-\Delta E}^{\Delta E} |\hat{\rho}(z,E) - \rho(z,E)| dE dz, \quad (8)$$

where each TCAV image was cleaned up by setting all pixel values below 50 to 0, and centered around the center of mass of the image. Feedback parameters and beam properties are summarized in Table I.

These preliminary results have demonstrated a new approach to controlling the longitudinal phase space of high energy, short, electron bunches. The major strength of this approach is that it is model independent, robust to noise, and can tune many coupled parameters simultaneously. The next step in this work will be to add more controlled parameters, and study the problem for several electron bunch charges and beam energies. The algorithm presented here is general, adjusting a high-dimensional parameter space based only on scalar "cost" value measurements and therefore can be useful for any large, complex system. PWFA facilities, such as the planned FACET-II, can benefit from the approach demonstrated here for creating custom shaped electron bunches.

This research was supported by Los Alamos National Laboratory's Laboratory-Directed Research and Development (LDRD) (Project No. 20180688ER) program and the SLAC National Accelerator Laboratory.

*ascheink@lanl.gov

[1] P. Emma, R. Akre, J. Arthur, R. Bionta, C. Bostedt, J. Bozek, A. Brachmann, P. Bucksbaum, R. Coffee, F. J. Decker, and Y. Ding, First lasing and operation of an ångstrom-wavelength free-electron laser, Nat. Photonics **4**, 641 (2010).

[2] Y. Ding, A. Brachmann, F. J. Decker, D. Dowell, P. Emma, J. Frisch, S. Gilevich, G. Hays, P. Hering, Z. Huang, and R. Iverson, Measurements and Simulations of Ultralow Emittance and Ultrashort Electron Beams in the Linac Coherent Light Source, Phys. Rev. Lett. **102**, 254801 (2009).

[3] D. Ratner, R. Abela, J. Amann, C. Behrens, D. Bohler, G. Bouchard, C. Bostedt, M. Boyes, K. Chow, D. Cocco, and F. J. Decker, Experimental Demonstration of a Soft X-Ray Self-Seeded Free-Electron Laser, Phys. Rev. Lett. **114**, 054801 (2015).

[4] C. Joshi, E. Adli, W. An, C. E. Clayton, S. Corde, S. Gessner, M. J. Hogan, M. Litos, W. Lu, K. A. Marsh, and W. B. Mori, Plasma wakefield acceleration experiments at FACET II, Plasma Phys. Controlled Fusion **60**, 034001 (2018).

[5] J. Rzepiela, H. Loos, R. Akre, A. Brachmann, F. J. Decker, Y. Ding, P. Emma, A. Fisher, J. Frisch, A. Gilevich, and P. Hering, Tuning of the LCLS Linac for User Operation, Report No. SLAC-PUB-16643, 2016.

[6] T. J. Maxwell, C. Behrens, Y. Ding, A. S. Fisher, J. Frisch, Z. Huang, and H. Loos, Coherent-Radiation Spectroscopy of Few-Femtosecond Electron Bunches Using a Middle-Infrared Prism Spectrometer, Phys. Rev. Lett. **111**, 184801 (2013).

[7] T. O. Raubenheimer, Technical challenges of the LCLS-II CW X-RAY FEL , in *Proceedings of the 6th International Particle Accelerator Conference, Richmond* (2015), http://accelconf.web.cern.ch/AccelConf/IPAC2015/papers/weyc1.pdf.

[8] A. A. Lutman, T. J. Maxwell, J. P. MacArthur, M. W. Guetg, N. Berrah, R. N. Coffee, Y. Ding, Z. Huang, A. Marinelli, S. Moeller, and J. C. Zemella, Fresh-slice multicolour X-ray free-electron lasers, Nat. Photonics **10**, 745 (2016).

[9] A. A. Lutman *et al.*, Femtosecond X-rays from Fresh-slice Multistage Free-Electron Lasers, Phys. Rev. Lett. (to be published).

[10] J. Amman, W. Berg, V. Blank, F. J. Decker, Y. Ding, P. Emma, Y. Feng, J. Frisch, D. Fritz, J. Hastings, and Z. Huang, Demonstration of self-seeding in a hard-X-ray free-electron laser, Nat. Photonics **6**, 693 (2012).

[11] D. Ratner *et al.*, Experimental Demonstration of a Soft X-Ray Self-Seeded Free-Electron Laser, Phys. Rev. Lett. **114**, 054801, 2015.

[12] V. Yakimenko, N. Lipkowitz, C. Clarke, M. Hogan, G. Yocky, C. Hast, S. Green, Y. Cai, N. Phinney, and G. White, FACET-II Accelerator Research with Beams of Extreme Intensities, in *Proceedings of IPAC2016, Busan, Korea*,

2016, http://accelconf.web.cern.ch/AccelConf/ipac2016/papers/tuobb02.pdf.

[13] A. Scheinker, Model independent beam tuning, in *Proceedings of the 2013 International Particle Accelerator Conference, Shanghai, China*, 2013, http://JACoW.org/IPAC2013/papers/tupwa068.pdf.

[14] A. Scheinker and D. Scheinker, Constrained extremum seeking stabilization of systems not affine in control, Int. J. Robust Nonlinear Control **28**, 568 (2018).

[15] A. Scheinker and S. Gessner, Adaptive method for electron bunch profile prediction, Phys. Rev. ST Accel. Beams **18**, 102801 (2015).

[16] N. Bruchon, G. Fenu, G. Gaio, M. Lonza, F. A. Pellegrino, and L. Saule, Free-electron laser spectrum evaluation and automatic optimization, Nucl. Instrum. Methods Phys. Res., Sect. A **871**, 20 (2017).

[17] C. Behrens, F. J. Decker, Y. Ding, V. A. Dolgashev, J. Frisch, Z. Huang, P. Krejcik, H. Loos, A. Lutman, T. J. Maxwell, and J. Turner, Few-femtosecond time-resolved measurements of X-ray free-electron lasers, Nat. Commun. **5**, 3762 (2014).

[18] A. L. Edelen, S. G. Biedron, B. E. Chase, D. Edstrom, S. V. Milton, and P. Stabile, Neural networks for modeling and control of particle accelerators, IEEE Trans. Nucl. Sci. **63**, 878 (2016).

[19] T. Tieleman and G. Hinton, COURSERA: Neural networks for machine learning, 4, 26–31, 2012, https://www.cs.toronto.edu/~tijmen/csc321/slides/lecture_slides_lec6.pdf.